

Hunt for dark subhalos in the galactic stellar field using computer vision

Mihael Petač^{*1,2}

¹*SISSA & INFN – Sezione di Trieste, Via Bonomea 265, 34136 Trieste, Italy*

²*Laboratoire Univers et Particules de Montpellier (LUPM) & CNRS & Université de Montpellier (UMR-5299), Place Eugène Bataillon, F-34095 Montpellier Cedex 05, France*

October 8, 2019

Abstract

The nature of dark matter remains uncertain despite several decades of dedicated experimental searches. The lack of tangible evidence for its non-gravitational interactions with ordinary matter gives good motivation for exploring new avenues of inferring its properties through purely gravitational probes. In particular, addressing its small-scale distribution could provide valuable new insights into its particle nature, either confirming the predictions of cold dark matter hypothesis or favouring models with suppressed small-scale matter power spectrum. In this work a machine learning technique for constraining the abundance of DM subhalos through the analysis of galactic stellar field is proposed. While the study is the first of its kind and hence applied only to a simplified synthetic datasets, the obtained results show promising potential for addressing the amount of DM substructure present within Milky Way. Using accurate astrometric observations, which became available only recently and are expected to rapidly improve in the near future, there is good hope to reach sensitivity needed for detecting DM subhalos with masses down to $10^7 M_{\odot}$.

1 Introduction

One of the characteristic predictions of the cold dark matter (CDM) paradigm is hierarchical growth of structure. According to it, the smallest objects collapsed under self-gravity first and subsequently underwent merging which led to the formation of increasingly large structures. This is supported by various observations, spanning scales from several Gpc down to a fraction of Mpc, giving an excellent match to the matter power spectrum predicted within the standard cosmological model [1, 2]. However, the study of dark matter (DM) distribution on sub-galactic scales turns out to be much more demanding since it requires extremely precise astronomical measurements as well as dealing with strongly non-linear regime of structure growth and baryonic processes. None-the-less, constraining the clustering properties of DM on small scales seems a promising way of obtaining new insights into the nature of DM particles, as many alternatives to the CDM hypothesis involve suppression small-scale matter power spectrum. Some of the most prominent suggestions of this type are warm [3–5], self-interacting [6] or fuzzy DM [7, 8]. At the same time, the signatures of galactic DM substructure can be searched for through purely gravitational effects, which have proven to be essential when addressing the phenomenon of DM. On the other hand, no convincing detection has been achieved so far through non-gravitational probes, such as direct and indirect searches or particle colliders, despite decades of efforts. However, it is important to note that a better understanding of sub-galactic DM

*petac@lupm.in2p3.fr

distribution could also help in improving the constraints on non-gravitational interactions between dark and visible sector, which could be achieved, for example, through better modelling of local DM distribution for direct detection experiments or discovering new prime targets for indirect searches.

Significant progress in addressing the DM clustering properties on small scales has been recently made through strong lensing observations, which are becoming sensitive to substructures down to $10^8 M_\odot$ [9, 10]. This is expected to improve even further in the near future with upcoming broad sky surveys [11, 12]. Similarly, valuable new astronomic observations opened novel opportunities for studying small-scale distribution of DM within the Milky Way. These range from searches for gravitationally bound groups of metal-poor stars [13–15], as was traditional done to identify ultra-faint dwarf satellite galaxies, to more recently proposed approaches, such as analysis of gaps in stellar streams left behind tidally disrupted objects [16, 17], searching for wakes in the distribution of Milky Way’s stars [18, 19] or detecting tidal heating of bound structures [20].

The aim of this work is to explore a novel technique for potential detection of dark galactic subhalos. Similarly to some of the approaches mentioned above, it relies on gravitational signatures of DM subhalos imprinted in the spatial and kinematic distribution of surrounding stars. As it was already noted in [18], subhalos with masses $M_{\text{sub}} \gtrsim 10^7 M_\odot$ should induce observable features in the phase-space distribution of galactic stellar field and with the recent release of Gaia’s astrometric data [21] it has become possible to search for them over a significant portion of our galactic neighbourhood. Additionally, new modern tools for reducing large and complex datasets have been developed, which allow us to go step further than the standard analyses used in the past. For the problem at hand perhaps the most interesting progress comes from the field of computer vision, where highly efficient convolutional neural network (CNN) models have been introduced, allowing for incredibly sophisticated extraction of information from image-like data – for a review on the topic see, e.g., [22, 23].

In section 2 we will begin with a short review of DM phenomenology that can be addressed through the study of DM substructure. In section 3 the possibility to detect signatures of dark subhalos in the galactic stellar field will be explored. After a brief presentation of the available datasets and some of their applications in the context of DM substructure, an analytical estimate for the detectability of perturbations induced by DM subhalos will be derived. This will be followed by a prescription of generating synthetic stellar fields, which are crucial for the training of neural network, and finally a concrete implementation of the CNN applicable to our problem will be presented. Section 4 contains several benchmarks of the advocated technique along with the corresponding discussion of our findings. Finally, a summary of our results and the outlook for future works is presented in section 5.

2 Particle properties encoded in small-scale structures

Non-linear gravitational clustering of cold and collisionless DM particles is expected to produce self-similar structures over a vast range of scales [24–28]. While the size of the largest perturbations is effectively set by the Hubble scale, their minimal size is in many models determined by the temperature of DM, establishing a scale below which the DM is expected to “free-stream”. On scales smaller than the free-streaming length any structure is expected to be washed out, which results in a sharp cut-off in the matter power spectrum. For standard WIMPs the details of thermal decoupling typically imply existence of DM subhalos at least down to $M_{\text{sub}} \sim 10^{-4} M_\odot$ [29, 30], which is much smaller than the foreseeable accuracy of astronomical measurements. On the other hand, in warm DM models the particles are assumed to decouple relativistic, which typically results in strong suppression of present matter power spectrum just below the scale of smallest dwarf galaxies. Therefore, in this case one does not expect to find abundant DM substructure within a galactic halo, which is in stark contrast with the CDM prediction. The small-scale matter power spectrum can also be modified in the case of DM particles with negligible thermal velocities. For example, non-thermally produced ultra-light bosons can be consistent with CDM predictions on large scales, but for masses $m_\chi \lesssim 10^{-22}$ eV the quantum effects start dominating their behaviour on distances of the order of kpc [7, 8]. The emergence of solitonic cores (i.e. condensates satisfying the ground state solution of the Schrödinger-Poisson equation) prohibits them from forming structures on scales smaller than

the corresponding de-Broglie wave-length, which in turn sets a minimal possible DM halo mass. For fermionic DM similar bounds can be derived by assuming that DM particles form a self-gravitating degenerate Fermi gas. In this case the Pauli exclusion principle prohibits the formation of arbitrarily dense structures, which again leads to a minimal possible halo mass for a given m_χ . As an example, from the existence of dwarf galaxies one can conclude that fermionic DM needs to have $m_\chi \gtrsim 100$ eV [31–33]. The small-scale properties of DM could also be affected by self-interactions within the dark sector. In particular, elastic scattering among DM particles would lead to formation of isothermal cores in regions with sufficiently high DM densities and inhibit further gravitational contraction. This would again result in a truncation of the matter power spectrum and absence of DM halos below certain scale. In this work, we will avoid addressing the vast range of possible scenarios that could be realized in nature – for example, a comprehensive framework for mapping different classes of particle physics models into the corresponding linear matter power spectrum has been formulated within the Effective Theory of Structure Formation (ETHOS) [34], while its non-linear evolution typically has to be studied by the means of numerical simulations. The only result that will be used through this work is the fact that many well motivated particle physics explanations of the DM phenomena lead to a significant suppression of the halo mass function at small scales, which can be used as an effective benchmark for excluding or favouring a particular class of models.

Besides the microphysics of DM, the abundance of galactic subhalos also crucially depends on their resilience against tidal disruption and violent baryonic processes. These effects are expected to be particularly important in the inner part of our galaxy, which is, however, of the prime interest for the presented analysis as it hosts the majority of galactic stars. Dedicated high-resolution numerical simulations suggest that cuspy DM subhalos can survive tidal shocks caused by the gravitational potential of host halo and baryonic disks [35–38], even though they lose the majority of their mass during the successive crossings of perihelion. Assuming CDM scenario, an estimate for the number of surviving subhalos in a Milky Way-like galaxy can be obtained using the semianalytical model recently suggested in [39]. Figure 1 shows the total number of subhalos with $M_{\text{sub}} \geq 10^7 M_\odot$ as a function of galactocentric distance for the aforementioned model for two extreme tidal disruption efficiencies (the latter is defined as the ratio between the corresponding tidal and scale radius, $\epsilon = r_t/r_s$, at which the object is considered as disrupted; “fragile subhalos” are defined to be disrupted when $\epsilon \leq 1$, while “resilient subhalos” remain bound until $\epsilon \leq 0.01$). According to this model, several cuspy subhalos with masses $M_{\text{sub}} \geq 10^7 M_\odot$ are expected to survive within the inner 20 kpc, regardless of the efficiency of tidal disruption. On the contrary, cored DM subhalos tend to be disrupted even much more easily and their abundance in disk galaxies is expected to be strongly suppressed within the inner 20 kpc – see, e.g., [40, 41], where unresolved central structure effectively makes the subhalos behave as cored [36, 38]. Consequently, the detection of sub-galactic DM structures would be a strong indicator in favour of CDM hypothesis, casting doubt on a wide range of alternative candidates, ranging from keV sterile neutrinos, ultra-light bosons to self-interacting DM models, which all predict DM cores. On the other hand, absence of the evidence for DM subhalos with masses $M_{\text{sub}} \gtrsim 10^7 M_\odot$ would be a compelling argument against the CDM paradigm. However, in this case robust conclusions would be much more difficult since only several of them are expected within the galactocentric distances that can be currently probed through the approach presented in this work.

3 A look at the galactic stellar field through computer vision

Recent Gaia’s second data release (DR2) [21] allows for unprecedented precision in the study of Milky Way’s stellar field. The improvements over previous catalogues are two-fold: firstly, it represents the largest dataset ever compiled, covering more than hundred million stars in our galactic neighbourhood, and secondly, it provides the most accurate global measurement of stellar positions and parallaxes, typically reducing the uncertainty by order of magnitude compared to older surveys. Therefore, Gaia data grants us a new window into the details of dynamics and evolution of our galaxy. While the entire catalogue provides positions and parallaxes for an overwhelming number of stars, for the purpose of

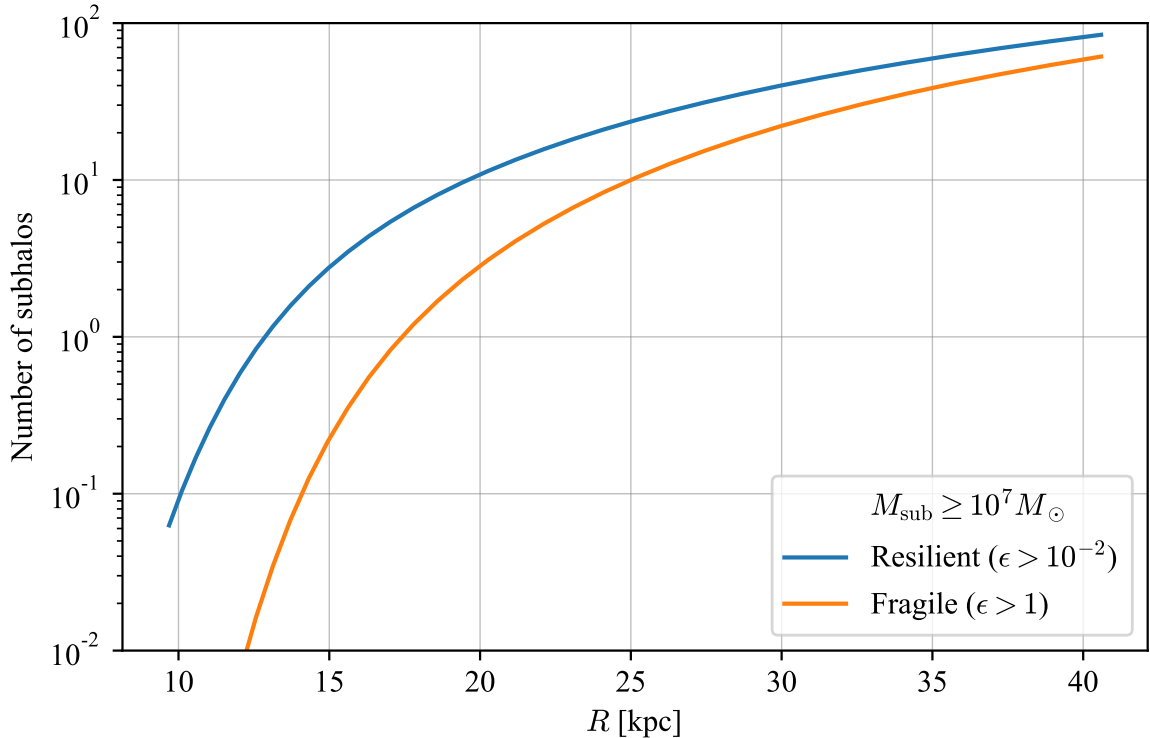


Figure 1: The expected number of surviving cuspy DM subhalos with $M_{\text{sub}} \geq 10^7 M_{\odot}$ in Milky Way-like galaxy as a function of galactocentric distance according to the semianalytical model of [39]. The blue line corresponds to subhalos which are highly resilient to tidal disruption effects (defined as bound until tidal radius reaches 1/100 of their scale radius, i.e. $\epsilon > 10^{-2}$), while the orange line shows the results for halos fragile subhalos (considered disrupted when the tidal radius becomes equal to halo’s scale radius, i.e. $\epsilon > 1$).

the presented analysis the full 6D phase-space information of the stellar field is needed. The latter is unfortunately available only for a subset of stars, for which also the radial velocities are determined. This amounts to roughly 7 million objects, most of which lie within 10 kpc of the Earth. These stars can be found in the official Gaia DR2 online archive ¹, but also in post-processed catalogues with explicitly computed galactocentric distances and velocities in the standard galactic coordinates, such as the ones provided by Marchetti et al. [42] or Sanders et al. [43], where the latter additionally combines Gaia DR2 astrometry and spectroscopic measurements of APOGEE, GALAH, LAMOST, RAVE and SEGUE.

While the importance of the Gaia mission for astrophysics has been well recognized, its possible implications for the studies of DM have received lesser attention. Interesting claims have been made in the context of Milky Way formation, by identifying several populations of stars that were most probably accreted through past mergers. Based on numerical simulations, it was argued that these stars should exhibit similar kinematic properties as the DM that was accreted along with them [44,45]. Apart from this, several attempts have been made to assess the amount of DM subhalos through the study of tidal streams left behind globular clusters [46,47]. However, such approaches had limited

¹<https://gea.esac.esa.int/archive/>

results since they are sensitive only to relatively small volume around the stream and, at the same time, perturbations very similar to the ones sourced by DM subhalos could be produced by various other galactic structures. In this section, we will explore the possibility of inferring information about DM substructure by means of full 6D stellar phase-space measurements. Such possibility was previously considered by Buschmann et al. [19]. However, their proposed analysis relies on the assumptions that DM subhalos have a cored Plummer density profile and that the surrounding stellar field is homogeneous with isotropic Gaussian velocity distribution, which are very restraining approximations. Instead, the approach advocated here is applicable to any stellar distribution, as well as an arbitrary DM density profile within the subhalos. Furthermore, in contrast with the work of Buschmann et al., which relied on likelihood-based analysis of the data, we will instead make use of the state-of-the-art computer vision tools, which allow for highly accurate extraction of features from extensive datasets at a relatively small computational cost. In particular, the ability of deep CNNs to recognize the characteristic subhalo-induced patterns in spatial and velocity distributions of stars will be explored. As it is typically the case in all practical applications of machine learning, the success crucially depends on the quality of training data. Since the results presented here are only the first step in the exploration of possibilities that CNNs offer in this particular context, only a simplified problem will be addressed, where additional perturbations of the stellar field due to, e.g., globular clusters or giant molecular clouds will be neglected. Furthermore, only homogeneous stellar field with Gaussian velocity distribution will be considered, however, a generalization to an arbitrary stellar distribution can be easily achieved.

In the following, we will first discuss the feasibility of detecting small perturbations in stellar kinematics sourced by DM substructures based on analytical estimates. This will be followed by a discussion of the algorithm for generating the mock realizations of the galactic stellar field in presence (or absence) of DM subhalos, which will serve as training data for the CNN. Finally, the details regarding our implementations of a simple classifier network, designed to detect the number of subhalos in a specific mass range within a sample dataset, are presented.

3.1 Detectability of subhalos

Exploring novel possibilities of studying the small-scale properties of DM seems a promising way of learning new insights regarding the nature of DM particle. Additional motivation for our endeavour comes from recent astronomic precision measurements, namely the astrometric data provided by the Gaia mission. There is a number of factors that determine whether the subtle patterns induced by DM substructure in stellar phase-space distribution can actually be found in observational datasets. Evidently, the mass of the subhalo plays a crucial role since it is directly proportional to the force exerted on surrounding stars. However, stellar number density and kinematic properties are also important, as they determine the sample size and noise level for studying the perturbations. Finally, when addressing real observations, one needs to take into account also measurement errors, which make convincing detections even more difficult.

To get an estimate of the gravitational perturbation caused by a DM subhalo, one can simply compute the variation in stellar kinetic energy in the vicinity of a compact clump with mass M_{sub} :

$$\delta T_{\text{sub}} = \frac{GM_{\text{sub}}}{\Delta r} \quad \text{with} \quad \Delta r^{-1} = r_{\text{min}}^{-1} - r_{\text{max}}^{-1}, \quad (1)$$

where r_{min} and r_{max} are the minimal and maximal distance of the considered star to the centre of subhalo, while G is the gravitational constant. To detect the perturbation of size δT the signal must be at least of the same order as the noise. Given a stellar population with velocity dispersion σ_* and typical measurement error δv_* , one can estimate the observational uncertainty in kinetic energy:

$$\delta T_{\text{obs}} \sim \sigma_* \cdot \delta v_*. \quad (2)$$

Since the velocities of individual stars are just random samples from their overall velocity distribution, not much can be learned from the trajectory of single star. Observations become useful only when nearby stars are binned together and local variations of kinematic properties are studied. This,

however, induces additional shot noise due to extracting average quantities from a finite sample. For a Gaussian distribution, one can show that the variance in the inferred velocity dispersion equals to:

$$\text{Var}(\sigma_*) = \frac{2\sigma_*^4}{N_b - 1}, \quad (3)$$

where N_b is the number of stars in a given bin. Therefore, by demanding that the signal is of the same order as the combined noise of measurement errors and binning in volume elements with characteristic length δr , one obtains:

$$\frac{GM_{\text{sub}}}{\delta r} \sim \sigma_* \cdot \delta v_* + \sigma_*^2 \cdot \sqrt{\frac{2}{N_b - 1}}, \quad (4)$$

$$\Rightarrow \hat{M}_{\text{sub}} \sim \frac{\sigma_* \cdot \delta r}{G} \left(\delta v_* + \sigma_* \sqrt{\frac{2}{N_b - 1}} \right). \quad (5)$$

The above expression provides an order-of-magnitude estimate for the minimum subhalo mass, \hat{M}_{min} , that could be detected in a particular catalogue of stars. Furthermore, from equation (5) one can also obtain an estimate for the optimal bin size δr in the corresponding stellar field with average mapped number density n_* :

$$\delta r \sim \left(\frac{\sigma_*}{\sqrt{2n_*} \delta v_*} \right)^{2/3}, \quad (6)$$

where the number of stars per bin was approximated by $N_b \approx n_* \cdot \delta r^3$. Note that for successful application of the suggested method δr must be appreciably smaller than extent of the mapped stellar field. Gaia's second data release provides us with accurate 6D phase-space measurements for several million stars within a radius of nearly 10 kpc from Earth, which amounts to average stellar density $n_* \sim 10^3 \text{ kpc}^{-3}$, with the accuracy of velocity measurements $\delta v_* \sim 5 \text{ km/s}$, while the typical velocity dispersion of galactic stars is in the range of $\sigma_* \sim 50 \text{ km/s}$. This implies:

$$\delta r \sim 0.4 \text{ kpc} \cdot \left(\frac{\sigma_*}{50 \text{ km/s}} \right)^{2/3} \left(\frac{\delta v_*}{5 \text{ km/s}} \right)^{-2/3} \left(\frac{n_*}{10^3 \text{ kpc}^{-3}} \right)^{-1/3}, \quad (7)$$

$$\hat{M}_{\text{min}} \sim 10^7 M_\odot \cdot \left(\frac{\sigma_*}{50 \text{ km/s}} \right)^{5/3} \left(\frac{n_*}{10^3 \text{ kpc}^{-3}} \right)^{-1/3} \left(\frac{\delta v_*}{5 \text{ km/s}} \right)^{1/3}. \quad (8)$$

As can be seen from the above estimates, there is good hope to detect DM subhalos with masses down to $10^7 M_\odot$ in the high quality data that has recently become available. Successful detection of a single subhalo in this mass range could rule out many alternatives to the cold DM hypothesis, while the absence of compelling signals would be harder to interpret due to large uncertainties in the expected abundance of subhalos and their distribution within the Milky Way. Fortunately, significant improvements in the coverage and accuracy of observations are expected with the future Gaia data releases [48], but also upon combining their results with other surveys such as the ones planned for LSST [12, 49] and other large telescopes [50]. On the other hand, from equation (8) one can see that the smallest detectable subhalo mass strongly depends on the σ_* and hence studying cold stellar populations, such as thin disk stars (or more accurately speaking, α -poor population), could lead to significantly lower \hat{M}_{sub} . However, this comes at the cost of reducing the probed region of the galaxy and hence lower probability to find a subhalo with $M_{\text{sub}} \gtrsim \hat{M}_{\text{sub}}$ in the considered volume, while the corresponding decrease in the number of tracer stars with respect to the entire catalogue should have a sub-dominant effect due to the weak (inverse cubic root) dependence of \hat{M}_{sub} on n_* .

3.2 Generation of mock data

In order to produce mock stellar field, which contains dark subhalos with known abundance and properties, there are several possible approaches. Buschmann et al. [19] derived an equilibrium distribution function for stars in the vicinity of a DM subhalo with Plummer density profile. However,

their solution assumes homogeneously distributed stars with isotropic Gaussian velocity distribution. For the task at hand, we will make use of a different approach, in which the distribution of stars can be adjusted to match the one inferred from observations. Such mock dataset can be constructed by dividing the observed volume of the galaxy in bins, where each of them is populated with stars following some net properties, namely the number density and velocity distribution corresponding to that location. These can be inferred from the observations, however, they need to be averaged over scales much larger than the expected size of DM perturbation in order to avoid including unknown structures in the synthetic stellar field. In practice, this can be achieved by binning the mapped stars in relatively large spatial bins and then smoothly interpolating the number density and moments of velocity distribution over a finer grid that is used for constructing the mock dataset. Such smoothed stellar field then needs to be endowed by DM substructure and its phase-space distribution updated according to the gravitational effects of the inserted subhalos. This can be done by beginning with specifying the subhalo position, \vec{r}_{sub} , velocity, \vec{v}_{sub} , and mass, M_{sub} . The latter allows one to determine the characteristic radius, r_g , at which the gravitational potential of the subhalo is comparable to the typical uncertainty in stellar velocity. Making use of the relation (4), one can define:

$$r_g \equiv \frac{GM_{\text{sub}}}{\sigma_* \left(\delta v_* + \sigma_* \sqrt{\frac{2}{N_b - 1}} \right)}, \quad (9)$$

which is to be used for determining whether a given star at position \vec{r}_* is considered as perturbed or the gravitational effects of the subhalo can be safely neglected. While such criterion guarantees that the change in stellar kinetic energy is below the typical measurement error, one could worry that there is a non-negligible effect on the direction of its velocity, if the star passed sufficiently close to the subhalo in the past. However, the probability for such a close encounter falls off as $(\vec{r}_* - \vec{r}_{\text{sub}})^{-2}$ and can also be safely neglected. On the other hand, stars that are within the characteristic radius (i.e. $|\vec{r}_* - \vec{r}_{\text{sub}}| < r_g$) receive non-negligible correction, which can be computed according to the standard results for scattering in a central potential. For each such star, one first has to determine the elapsed time, t_0 , and the corresponding position, $\vec{r}_{0,*}$, since entering the radius of influence:

$$|\vec{r}_{\text{rel}} + t_0 \cdot \vec{v}_{\text{rel}}| = r_g \quad \text{where} \quad \vec{r}_{\text{rel}} = \vec{r}_* - \vec{r}_{\text{sub}} \quad \text{and} \quad \vec{v}_{\text{rel}} = \vec{v}_* - \vec{v}_{\text{sub}}$$

$$\Rightarrow \vec{r}_{0,*} = \vec{r}_* - t_0 \cdot \vec{v}_*, \quad (10)$$

$$t_0 = \frac{1}{v_{\text{rel}}^2} \left(\vec{r}_{\text{rel}} \cdot \vec{v}_{\text{rel}} \pm \sqrt{(\vec{r}_{\text{rel}} \cdot \vec{v}_{\text{rel}})^2 + v_{\text{rel}}^2 (r_g^2 - r_{\text{rel}}^2)} \right). \quad (11)$$

From the point $\vec{r}_{0,*}$ one can then compute the stellar trajectory under the influence of subhalo's gravitational potential $\Phi(r)$. For spherically symmetric potentials problem can be simplified by moving to the scattering plane, where the trajectory becomes two dimensional and can be described in terms of the azimuthal angle ϕ and time t as a function of radial distance r (i.e. distance from the centre of the potential) [51]:

$$\phi(r) = b \int_{r_{\text{min}}}^r \frac{dx}{x^2 \sqrt{1 - b^2/x^2 + \Psi(x)}}, \quad (12)$$

$$t(r) = \frac{1}{|\vec{v}_* - \vec{v}_{\text{sub}}|} \int_{r_{\text{min}}}^r \frac{dx}{\sqrt{1 - b^2/x^2 + \Psi(x)}}, \quad (13)$$

$$\text{where } b = |\vec{r}_{0,*} \times \vec{v}_{\text{rel}}| / |\vec{v}_{\text{rel}}| \quad \text{and} \quad r_{\text{min}} = \frac{GM_{\text{sub}}}{v_{\text{rel}}^2} \left(\sqrt{1 + \left(\frac{b v_{\text{rel}}^2}{GM_{\text{sub}}} \right)^2} - 1 \right)$$

are the impact parameter and the distance of closest approach, respectively. By evaluating these expressions for the elapsed time since entering in the gravitational range, r_g , and mapping it back to the galactic coordinate frame, one can then determine the actual position and velocity of each

perturbed star. For a Keplerian potential (i.e. subhalos approximated by a point-mass) the above integrals admit an analytical solution, while the modified stellar positions and velocities can be obtained numerically for an arbitrary spherical gravitational potential. Additionally, this procedure of synthesizing the Milky Way stellar field is robust against the inhomogeneities in fiducial distribution, provided that they correspond to scales sufficiently larger than r_g . Furthermore, it is also capable of accounting for spacial dependence of the stellar velocity distribution, which does not need to be Gaussian nor isotropic. Note that none of these features are possible in the analytical approach discussed in [19]. In the following, however, the simplified case of homogeneous stellar field with Gaussian velocity distribution will be considered for the sake of comparing the generated datasets to the analytical solution. An example of the produced dataset is presented in figure 2, along with predictions of the analytical model. As can be seen from the plots, qualitative features in the obtained stellar density and averaged velocities are very similar, despite very different methods used to generate the maps.

Addressing the actual stellar field, as mapped by Gaia satellite, is a complex task. Besides non-trivial position-dependent phase-space distribution of stars, the data contains numerous features which are most probably not sourced by DM substructure, such as spiral arms, globular clusters, giant molecular clouds, etc. Therefore, in the first step of applying computer vision for detecting DM subhalos, we focused on a simplified case, assuming homogeneous stellar field with Gaussian velocity distribution and neglect the possibility of non-DM induced perturbations. Relaxing these assumptions naturally requires much more careful generation of training data, but also makes the extraction of DM signatures more difficult. However, the perturbations induced by DM substructure are fortunately rather unique and can not be easily mimicked by any other galactic structures or perturbers due to the expected spheroidal morphology and high central density of the surviving DM subhalos. In principle, this makes it possible for the CNNs to distinguish them even in presences of other phase-space features over the scales of interest, but to obtain quantitative results for such realistic datasets further improvements in the generation of mock stellar fields will be needed. Furthermore, non-DM induced perturbations could also be excluded by a combination relevant complementary observations. For example, globular clusters should be detectable through accurate photometric studies, while the presence of giant molecular clouds could be inferred from the associated microwave emissions.

3.2.1 Search for DM subhalo signatures using CNN

Identifying gravitational perturbations induced by DM subhalos traversing the stellar field turns out to be a rather complicated task. The observations, as well as faithful mocks, form a 6D phase-space populated with millions of individual stars. There are several possible approaches for detecting subtle patterns in such datasets. In astronomy, the wavelet transform was probably one of the most extensively used techniques and represents the standard tool for identifying globular clusters and dwarf satellite galaxies from photometric images, see, e.g., [52–54]. However, as such it is sensitive only to stellar number density. Another possibility are algorithms designed to detect clusters in the higher-dimensional parameter spaces, e.g., Gaussian mixture model or its refined variations, such as extreme deconvolution algorithm [55]. While such analyses are mathematically well understood, it is less clear that the identified cluster of data points will actually correspond to stars perturbed by DM subhalo and additional modelling assumptions and data pruning is often required. Alternatively, when an accurate phase-space model for the distribution of stars in vicinity of the perturber is available, one can construct a likelihood function that is used to infer whether the sought after signal is present in the binned phase-space distribution of stars, as was done in [19]. While this approach can be quite effective in a simplified setup, the number of parameters needed for accurate modelling of the signals grows dramatically when considering real data, which makes its applicability questionable. On the other hand, modern techniques of machine learning have recently lead to major advances in the analysis of such high-dimensional datasets. For the task at hand, CNNs are particularly convenient as they are highly efficient for detecting characteristic features in noisy input data and posses a very useful property of translational invariance (for recent reviews of CNNs see, e.g., [22,23]). Furthermore, the machine learning algorithms use training data to teach themselves what are the relevant patterns and the user is only required to prepare representative training datasets, which is

in the case of galactic stellar field much simpler than constructing accurate parametric models. As an additional benefit, machine learning approach is much less computationally demanding and many highly optimized implementations of deep neural networks are publicly available.

The CNN used in this study is constructed in such a way that it takes stellar number density distribution and first two moments of the velocity distribution as its input and returns the probabilities for a given dataset to contain a certain number of subhalos. Since not more than a few detectable DM clumps (i.e. subhalos with mass greater than \hat{M}_{sub}) are expected within the portion of galaxy mapped by Gaia, one can use a classifier network with only a several output classes, where each of them corresponds to a fixed number of subhalos contained in the given volume. On the other end of the network, the input data comprises of seven 3D grids, which can be from the machine learning perspective interpreted as 3D images, and correspond to spatially binned information regarding the stellar number density, as well as average velocities and velocity dispersions along the three coordinate axes. These seven grids are referred to as channels since in the conventional application of CNNs they usually represent different colour channels of the image. An especially useful feature of CNNs is the fact that they simultaneously cross-correlate the signals at a given spatial position in the image across all the channels, which results in surprisingly high sensitivity for the characteristic patterns exhibited by the stellar field perturbed by the DM subhalos. Furthermore, the translational invariance of CNNs greatly reduces the number of required training samples, since the spatial position of signals becomes irrelevant, and the network is automatically capable of recognizing it anywhere within the grid. Besides just extracting the number of dark subhalos in a given dataset, there is good hope to transform the described neural network from a classifier into a regression model, able of quantifying the mass of perturber, as well as its location and velocity. However, in this preliminary study I will consider only the simpler case of classification network, since regression models can be constructed only for a known fixed number of embedded subhalos and would, therefore, serve as second step in the analysis of data.

The above network was constructed through Python implementation of Keras library [56]. It uses 3D convolutional layers, each followed by batch normalization, drop-out and max-pooling layer, which then connect to final dense layers. Each convolutional layer contains a number of filters, which are trained to produce positive signals when convoluted with the part of the stellar field that contains the sought-after pattern. By stacking multiple convolution layers, one increases the robustness and the range of features that can be learned. The subsequent normalization and drop-out layers are used to assure effective training, while the max-pooling is used to reduce the amount of data passing through each step of convolution. The latter is necessary in order to end up with a manageable amount of weights in the dense layers, which are responsible for final classification of the inputs. Precise summary of the network layout is presented in table 1. For training of the network Keras implementation ADAM optimizer with learning rate $\text{lr} = 10^{-4}$ was used, along with the categorical cross-entropy metric. 20% of the input samples served as a validation set, while the rest 80% was used for training.

4 Results

As already stated above, the scope of this preliminary study was limited to homogenous stellar field with Gaussian velocity distribution. In such setting each dataset can be fully characterized by the number of embedded subhalos, their masses and velocities, and additionally the stellar number density and velocity dispersions along with the three spatial directions. A sample realization of the stellar field containing a single DM subhalo with $M_{\text{sub}} = 10^7 M_{\odot}$, which is moving in positive \hat{x} direction with $|\vec{v}_{\text{sub}}| = 100$ km/s through stellar field with $n_{\star} = 10^3$ kpc $^{-3}$ and $\sigma_{\star,x} = \sigma_{\star,y} = \sigma_{\star,z} = 10$ km/s, is shown in figure 3. As can be seen, the features induced by the presence of DM subhalo are very subtle and nearly impossible to spot by eye.

To test the efficiency of CNNs in extracting the number of subhalos in a given stellar field, we first generated 32000 training samples, which contained between 0 and 2 point-mass subhalos with $M_s = 10^7 M_{\odot}$ and velocity drawn from isotropic Gaussian distribution with $\sigma_{\text{sub}} = 50$ km/s. The stars were then binned in 22 bins per spatial dimension and corresponding 3D maps of number density

Layer	Output shape	Number of parameters
Conv3D	(20,20,20,32)	6080
BatchNormalization	(20,20,20,32)	80
Dropout	(20,20,20,32)	0
MaxPooling	(10,10,10,64)	0
Conv3D	(8,8,8,32)	27680
BatchNormalization	(4,4,4,32)	16
Dropout	(20,20,20,32)	0
MaxPooling	(4,4,4,32)	0
Flatten	64	0
Dense	64	131136
Dense	32	2080
Dense	3	99

Table 1: Simple CNN used for classifying the amount of DM subhalos in a give stellar field. The expected inputs are seven $22 \times 22 \times 22$ grids, containing the spacial information regarding the stellar number density and the three components of the first two moments of the velocity distribution. In total the model has 167091 trainable parameters.

and velocity moments were created. Finally, the obtained maps were used to train the CNN, which typically took about 20 epochs (i.e. iterations through the entire set of maps). The network’s loss function and accuracy versus the number of training epochs are shown in figure 4. Once the training of network converged, we used it to extract the number of subhalos from a collection of independent stellar field realization, which was not used in the training procedure, serving as a test dataset. The network reached an accuracy of more than 99.9%, miss-classifying one sample out of several thousand.

With decreasing M_{sub} , it becomes increasingly difficult to detect the signatures of substructure, since both, the magnitude of perturbations and number of stars effected by it, decrease. However, after repeating the training procedure with stellar fields containing subhalos with $M_{\text{sub}} = 5 \cdot 10^6 M_{\odot}$ the network reached only slightly worse accuracy of 99.8%. Similar results were found for $M_{\text{sub}} = 3 \cdot 10^6 M_{\odot}$, while the network failed to train when $M_{\text{sub}} \lesssim 2 \cdot 10^6 M_{\odot}$. The efficiency of CNNs to recognize substructure of a given mass is nicely captured in receiver operating characteristic (ROC) curves, measuring the rate of correct classification versus the rate of false classifications as the threshold value of signal needed for assigning it to a certain category is being varied. They are shown in figure 5 for networks trained with datasets containing aforementioned mono-chromatic subhalo masses, as well as a network trained on dataset with uniformly distributed subhalo masses in the range $M_{\text{sub}} \in [3 \cdot 10^6, 10^7] M_{\odot}$, which is a step closer to the realistic setting, since galactic DM substructures are expected to vary in mass. As can be seen from the plot, CNN performed well in all the cases where $M_{\text{sub}} \geq 3 \cdot 10^6 M_{\odot}$, yielding the worst performance for datasets with varying subhalo masses, but still reaching decent accuracy of 97.1%. Interestingly enough, the network was not able to train on datasets with $M_{\text{sub}} < 3 \cdot 10^6 M_{\odot}$ and exhibited a behaviour reminiscent of a phase-transition, reaching precision better than 97% above the aforementioned threshold value of M_{sub} and failed to train below it.

To further explore the dependence of subhalo detection efficiency on the M_{sub} , but also stellar parameters, we trained CNNs for several combinations of $M_{\text{sub}}/\sigma_{\star}^2$, characterizing the relative strength of the perturbation, and n_{\star} , determining noisiness of the binned data. Results are shown in figure 6, where the green crosses mark parameter values at which network trained successfully, reaching accuracy above 95%, and red crosses where it failed, resulting in accuracy $\sim 33\%$, which equals to random guessing between the three possible answers regarding the number of contained subhalos. In the same plot also the sensitivity threshold estimate from equation (4) is shown, where δv_{\star} was set to 0 since

the mock datasets did not include measurement uncertainties of the stellar velocities ². As can be seen from the figure 6, the derived estimate leads to better expected sensitivity than the one found in practice, which implies that the perturbations in stellar distribution need to be somewhat larger than the shot noise induced by binning of the stars, in order for the CNN do detect them. At intermediate values of $GM_{\text{sub}}/\sigma_{\star}^2 \sim 0.2$, for which the δr that was used for binning the stellar field is near the optimal choice, a correction factor in \hat{M}_{sub} of less than 2 is needed. However, the discrepancy gets more severe at larger and smaller values of $GM_{\text{sub}}/\sigma_{\star}^2$. This could be perhaps mitigated by choosing more appropriate δr , but that would also imply changing either the sizes of network layers or the considered stellar field volume.

Finally, also the case of anisotropic stellar velocity distributions was explored by setting different velocity dispersions along the three spatial directions. In this case, we found that the sensitivity mostly depends on the smallest velocity dispersion component, chosen as $\sigma_{\star,z}$, yielding only slightly worse accuracy than in isotropic setting with the same velocity dispersion along all three spatial components, i.e. $\sigma_{\star} \sim \sigma_{\star,z}$. The exact allowed increase in stellar velocity dispersion components perpendicular to $\sigma_{\star,z}$, for which still a classification with accuracy greater than 95% could be achieved, was found to be non-trivially dependent on n_{\star} and M_{sub} , but typically exceeded a factor of 2. This result is particularly important for the application of the discussed technique to real data, as it tells us that it is probably best to look for the perturbations in thin disk stars, which are typically characterized by small velocity dispersion in the direction perpendicular to the galactic disk, allowing for detection of significantly smaller M_{sub} than through thick disk and/or halo stars.

5 Conclusions

In our work we examined a novel method for constraining the abundance of dark subhalos through the study of galactic stellar field using machine learning tools. Astrometric data of adequate quality for such analyses has only recently become available, however, in the near future even more extensive and accurate catalogues are expected to be released. This opens a new window for the studies of DM distribution on the sub-galactic scales, which could contain valuable hints regarding the nature of DM particles. The presented analysis was performed on simplified synthetic stellar fields, where only perturbations in the stellar phase-space distribution sourced by DM subhalos were considered. For such setup an empirical bound for detectability of dark subhalos through the use of CNNs was obtained – see figure 6. Our findings show that the minimal detectable subhalo mass is only by factor of a few above the derived analytical estimate (5), which assumes that strength of the signal equals to the intrinsic uncertainty of the data. This gives good hope that astrometric observations provided by Gaia mission could be used for finding dark subhalos with masses down to the order of $10^7 M_{\odot}$. It was also demonstrated that CNNs are almost equally efficient for recognizing patterns induced by mono-chromatic and extended DM subhalo masses, which is a very useful feature when addressing real observations. For detection of the smallest subhalos cold stellar populations, namely the ones with small velocity dispersion at least in one spatial component, were recognized as particularly important. A prime candidate are perhaps the galactic α -poor stars, since they exhibit very low velocity dispersion perpendicular to the galactic disk. On the other hand, before being able to analyse actual observations, significant improvements are still needed in the generation of mock stellar catalogues to include possible features which are not sourced by DM substructure. Nuisance signals might arise, for example, from globular clusters, giant molecular clouds, spiral arms or other galactic structures. While there is good hope for CNNs to distinguish them from subhalo-induced phase-space patterns, this still needs to be confirmed through future tests. Furthermore, the trajectories of perturbed stars in our procedure of generating mock datasets might be additionally effected by other sources of gravitational potential with non-negligible gradient on the scale of interest. There are also several possible improvement of the presented analysis. Increased sensitivity could be perhaps

²It turns out that the errors in velocity measurements provided by Gaia data are subdominant and the shot noise due to binning dominates the uncertainty in inferred moments of stellar velocity distribution. An exception to this is perhaps the stellar field within a fraction of kpc distance from Earth, where the mapped number density of stars is extremely high.

achieved by considering a projection of the stellar motion on the sky sphere since this would allow one to use the entire Gaia dataset, without restricting only to a subset of stars with determined radial motions. However, it is not clear that this approach would necessarily result in better accuracy, because stars with only 5D astrometric data carry less information and are typically associated much larger observational uncertainties in the measured parallaxes and proper motions. Further improvements might also be possible on the side of the deployed neural network model, e.g., by using larger number layers or different network topologies. In future research it would also be very interesting to explore the possibilities of applying regression CNNs for extracting the mass, location and velocity of a given subhalo.

Acknowledgments

I would like to thank Gabriëla Zaharijas and Christopher Eckner for many stimulating debates during the preparation of this work. Additionally, I am very grateful to Christopher for devoting his valuable time in exploration of alternatives to the machine learning approach. The latter unfortunately turned out to be much more demanding than initially thought and their comparison with the method presented here falls well beyond the scope of this work. Special credit for providing his results regarding the expected number of cuspy subhalos in Milky Way-like galaxy goes to Gaëtan Facchinetti. I would also like to thank the Dark Machines initiative for providing support and enabling the exchange of knowledge between physics and machine learning communities. The author acknowledges partial support from the European Union’s Horizon 2020 research and innovation programme under the Marie Skłodowska-Curie grant agreements No 690575 and 674896, as well as the ANR project ANR-18-CE31-0006.

References

- [1] Planck Collaboration, N. Aghanim, Y. Akrami, et al. Planck 2018 results. VI. Cosmological parameters. *arXiv e-prints*, page arXiv:1807.06209, July 2018.
- [2] Solène Chabanier, Marius Millea, and Nathalie Palanque-Delabrouille. Matter power spectrum: from Ly α forest to CMB scales. *Monthly Notices of the Royal Astronomical Society*, 489(2):2247–2253, October 2019.
- [3] Scott Dodelson and Lawrence M. Widrow. Sterile neutrinos as dark matter. *Physical Review Letters*, 72(1):17–20, January 1994.
- [4] Paul Bode, Jeremiah P. Ostriker, and Neil Turok. Halo Formation in Warm Dark Matter Models. *The Astrophysical Journal*, 556(1):93–107, July 2001.
- [5] Dan Hooper, Manoj Kaplinghat, Louis E. Strigari, and Kathryn M. Zurek. MeV dark matter and small scale structure. *Physical Review D*, 76(10):103515, November 2007.
- [6] Sean Tulin and Hai-Bo Yu. Dark Matter Self-interactions and Small Scale Structure. *Physics Reports*, 730:1–57, February 2018.
- [7] Wayne Hu, Rennan Barkana, and Andrei Gruzinov. Fuzzy Cold Dark Matter: The Wave Properties of Ultralight Particles. *Physical Review Letters*, 85(6):1158–1161, August 2000.
- [8] Lam Hui, Jeremiah P. Ostriker, Scott Tremaine, and Edward Witten. Ultralight scalars as cosmological dark matter. *Physical Review D*, 95(4):043541, February 2017.
- [9] Simona Vegetti and L. V. E. Koopmans. Statistics of mass substructure from strong gravitational lensing: quantifying the mass fraction and mass function. *Monthly Notices of the Royal Astronomical Society*, 400(3):1583–1592, December 2009.
- [10] D. Bayer, S. Chatterjee, L. V. E. Koopmans, et al. Observational constraints on the sub-galactic matter-power spectrum from galaxy-galaxy strong gravitational lensing. 2018.

- [11] Tansu Daylan, Francis-Yan Cyr-Racine, Ana Diaz Rivero, Cora Dvorkin, and Douglas P. Finkbeiner. Probing the Small-scale Structure in Strongly Lensed Systems via Transdimensional Inference. *The Astrophysical Journal*, 854(2):141, February 2018.
- [12] Keith Bechtol, Alex Drlica-Wagner, Kevork N. Abazajian, et al. Dark Matter Science in the Era of LSST. *arXiv:1903.04425 [astro-ph, physics:hep-ex]*, March 2019.
- [13] V. Belokurov, D. B. Zucker, N. W. Evans, et al. Cats and Dogs, Hair and a Hero: A Quintet of New Milky Way Companions*. *The Astrophysical Journal*, 654(2):897, January 2007.
- [14] K. Bechtol, A. Drlica-Wagner, E. Balbinot, et al. Eight new milky way companions discovered in first-year dark energy survey data. *The Astrophysical Journal*, 807(1):50, June 2015.
- [15] Joshua D. Simon. The Faintest Dwarf Galaxies. *arXiv:1901.05465 [astro-ph]*, January 2019. arXiv: 1901.05465.
- [16] Denis Erkal and Vasily Belokurov. Properties of dark subhaloes from gaps in tidal streams. *Monthly Notices of the Royal Astronomical Society*, 454(4):3542–3558, December 2015.
- [17] Nilanjan Banik, Gianfranco Bertone, Jo Bovy, and Nassim Bozorgnia. Probing the nature of dark matter particles with stellar streams. *Journal of Cosmology and Astroparticle Physics*, 2018(07):061–061, July 2018.
- [18] Robert Feldmann and Douglas Spolyar. Detecting dark matter substructures around the Milky Way with Gaia. *Monthly Notices of the Royal Astronomical Society*, 446(1):1000–1012, January 2015.
- [19] Malte Buschmann, Joachim Kopp, Benjamin R. Safdi, and Chih-Liang Wu. Stellar Wakes from Dark Matter Subhalos. *Physical Review Letters*, 120(21):211101, May 2018.
- [20] Jorge Peñarrubia. Stochastic tidal heating by random interactions with extended substructures. *Monthly Notices of the Royal Astronomical Society*, 484(4):5409–5436, April 2019.
- [21] L. Lindegren, J. Hernández, A. Bombrun, et al. Gaia Data Release 2 - The astrometric solution. *Astronomy & Astrophysics*, 616:A2, August 2018.
- [22] Yong Ren and Xuemin Cheng. Review of convolutional neural network optimization and training in image processing. In *Tenth International Symposium on Precision Engineering Measurements and Instrumentation*, volume 11053, page 1105331. International Society for Optics and Photonics, March 2019.
- [23] Waseem Rawat and Zenghui Wang. Deep Convolutional Neural Networks for Image Classification: A Comprehensive Review. *Neural Computation*, 29(9):2352–2449, June 2017.
- [24] J. A. Fillmore and P. Goldreich. Self-similar gravitational collapse in an expanding universe. *The Astrophysical Journal*, 281:1–8, June 1984.
- [25] E. Bertschinger. Self-similar secondary infall and accretion in an Einstein-de Sitter universe. *The Astrophysical Journal Supplement Series*, 58:39–65, May 1985.
- [26] Julio F. Navarro, Carlos S. Frenk, and Simon D. M. White. A Universal Density Profile from Hierarchical Clustering. *The Astrophysical Journal*, 490(2):493–508, December 1997.
- [27] James E. Taylor and Julio F. Navarro. The Phase-Space Density Profiles of Cold Dark Matter Halos. *The Astrophysical Journal*, 563(2):483, December 2001.
- [28] C. Alard. Dark matter haloes and self-similarity. *Monthly Notices of the Royal Astronomical Society*, 428(1):340–348, January 2013.
- [29] Anne M. Green, Stefan Hofmann, and Dominik J. Schwarz. The first WIMPy halos. *Journal of Cosmology and Astroparticle Physics*, 2005(08):003–003, August 2005.
- [30] Torsten Bringmann and Stefan Hofmann. Thermal decoupling of WIMPs from first principles. *Journal of Cosmology and Astroparticle Physics*, 2007(04):016–016, April 2007.
- [31] Valerie Domcke and Alfredo Urbano. Dwarf spheroidal galaxies as degenerate gas of free fermions. *Journal of Cosmology and Astroparticle Physics*, 2015(01):002–002, January 2015.

- [32] Lisa Randall, Jakub Scholtz, and James Unwin. Cores in dwarf galaxies from Fermi repulsion. *Monthly Notices of the Royal Astronomical Society*, 467(2):1515–1525, May 2017.
- [33] Chiara Di Paolo, Fabrizio Nesti, and Francesco L. Villante. Phase-space mass bound for fermionic dark matter from dwarf spheroidal galaxies. *Monthly Notices of the Royal Astronomical Society*, 475(4):5385–5397, April 2018.
- [34] Francis-Yan Cyr-Racine, Kris Sigurdson, Jesús Zavala, et al. ETHOS—an effective theory of structure formation: From dark particle physics to the matter distribution of the Universe. *Physical Review D*, 93(12):123527, June 2016.
- [35] Jorge Peñarrubia and Andrew J. Benson. Effects of dynamical evolution on the distribution of substructures. *Monthly Notices of the Royal Astronomical Society*, 364(3):977–989, December 2005.
- [36] Frank C. van den Bosch and Go Ogiya. Dark matter substructure in numerical simulations: a tale of discreteness noise, runaway instabilities, and artificial disruption. *Monthly Notices of the Royal Astronomical Society*, 475(3):4066–4087, April 2018.
- [37] Go Ogiya, Frank C. van den Bosch, Oliver Hahn, et al. DASH: a library of dynamical subhalo evolution. *arXiv:1901.08601 [astro-ph]*, January 2019.
- [38] Raphaël Errani and Jorge Peñarrubia. Can tides disrupt cold dark matter subhaloes? *arXiv:1906.01642 [astro-ph]*, June 2019.
- [39] Martin Stref, Thomas Lacroix, and Julien Laval. Remnants of Galactic subhalos and their impact on indirect dark matter searches. *arXiv:1905.02008 [astro-ph, physics:hep-ph]*, May 2019.
- [40] Till Sawala, Pauli Pihajoki, Peter H. Johansson, et al. Shaken and stirred: the Milky Way’s dark substructures. *Monthly Notices of the Royal Astronomical Society*, 467(4):4383–4400, June 2017.
- [41] Tyler Kelley, James S. Bullock, Shea Garrison-Kimmel, et al. Phat ELVIS: The inevitable effect of the Milky Way’s disc on its dark matter subhaloes. *Monthly Notices of the Royal Astronomical Society*, 487(3):4409–4423, August 2019.
- [42] T. Marchetti, E. M. Rossi, and A. G. A. Brown. Gaia DR2 in 6d: Searching for the fastest stars in the Galaxy. *Monthly Notices of the Royal Astronomical Society*.
- [43] Jason L. Sanders and Payel Das. Isochrone ages for ~ 3 million stars with the second Gaia data release. *Monthly Notices of the Royal Astronomical Society*, 481(3):4093–4110, December 2018.
- [44] Jonah Herzog-Arbeitman, Mariangela Lisanti, Piero Madau, and Lina Necib. Empirical Determination of Dark Matter Velocities Using Metal-Poor Stars. *Physical Review Letters*, 120(4):041102, January 2018.
- [45] Lina Necib, Mariangela Lisanti, Shea Garrison-Kimmel, et al. Under the Firelight: Stellar Tracers of the Local Dark Matter Velocity Distribution in the Milky Way. October 2018.
- [46] Denis Erkal, Vasily Belokurov, Jo Bovy, and Jason L. Sanders. The number and size of subhalo-induced gaps in stellar streams. *Monthly Notices of the Royal Astronomical Society*, 463(1):102–119, November 2016.
- [47] Nilanjan Banik and Jo Bovy. Effects of baryonic and dark matter substructure on the Pal 5 stream. *Monthly Notices of the Royal Astronomical Society*, 484(2):2009–2020, April 2019.
- [48] Gerard Gilmore. Gaia: 3-dimensional census of the Milky Way Galaxy. *Contemporary Physics*, 59(2):155–173, April 2018.
- [49] Alex Drlica-Wagner, Yao-Yuan Mao, Susmita Adhikari, et al. Probing the Fundamental Nature of Dark Matter with the Large Synoptic Survey Telescope. *arXiv:1902.01055 [astro-ph, physics:hep-ex, physics:hep-ph]*, February 2019.
- [50] Joshua Simon, Simon Birrer, Keith Bechtol, et al. Testing the Nature of Dark Matter with Extremely Large Telescopes. *Bulletin of the American Astronomical Society*, 51(3):153, May 2019.

- [51] Lev Davidovič Landau, Evgenij M. Lifšic, and Lev Davydovich Landau. *Mechanics*. Number by L. D. Landau and E. M. Lifshitz ; Vol. 1 in Course of theoretical physics. Elsevier, Butterworth Heinemann, Amsterdam [u.a], 3. ed., reprinted edition, 2007. OCLC: 254579166.
- [52] G. Coupinot, J. Hecquet, M. Auriere, and R. Futaully. Photometric analysis of astronomical images by the wavelet transform. *Astronomy and Astrophysics*, 259:701, June 1992.
- [53] Jean-Luc Starck. Multiscale Methods in Astronomy: Beyond Wavelets. *Astronomical Data Analysis Software and Systems XI*, 281:391, 2002.
- [54] Teresa Antoja, Cecilia Mateu, Luis Aguilar, et al. Detection of satellite remnants in the Galactic Halo with Gaia III. Detection limits for Ultra Faint Dwarf Galaxies. *Monthly Notices of the Royal Astronomical Society*, 453(1):541–560, October 2015.
- [55] Jo Bovy, David W. Hogg, and Sam T. Roweis. Extreme deconvolution: Inferring complete distribution functions from noisy, heterogeneous and incomplete observations. *The Annals of Applied Statistics*, 5(2B):1657–1677, June 2011.
- [56] François Chollet et al. *Keras*. 2015.

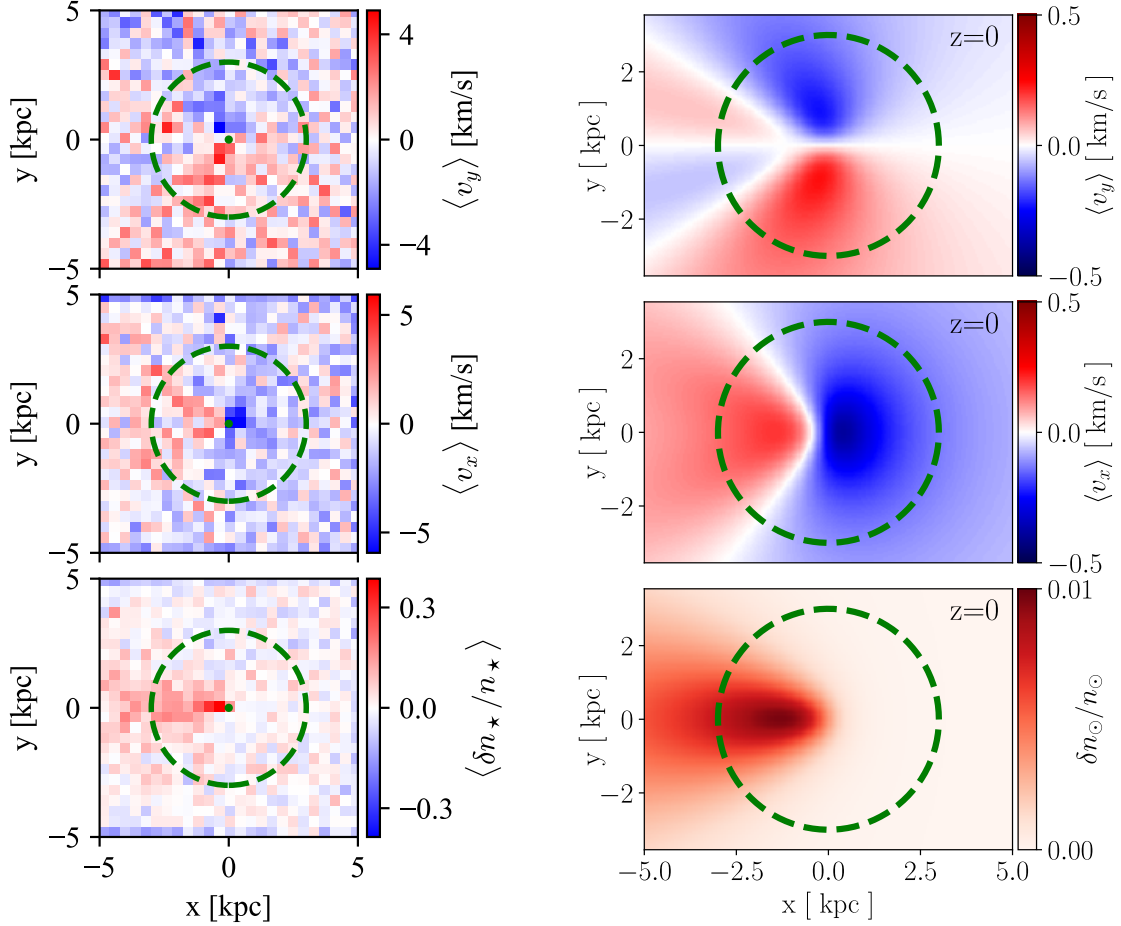


Figure 2: Stellar number density perturbation, $\langle \delta n_\star / n_\star \rangle$, and average velocities perpendicular, $\langle v_y \rangle$, and parallel, $\langle v_x \rangle$, to the subhalo's movement direction. In the plots on left hand side, generated according to the procedure described section 3.2, DM subhalo is assumed to have a mass of $M_{\text{sub}} = 5 \cdot 10^7 M_\odot$ and $|\vec{v}_{\text{sub}}| = 100$ km/s along \hat{x} direction, while for stars $n_\star = 10^4$ kpc $^{-3}$ and $\sigma_x = \sigma_y = \sigma_z = 30$ km/s were chosen. On the right hand side the results obtained by Buschmann et al. [19] using the analytical expression are shown, with the difference that $M_{\text{sub}} = 2 \cdot 10^7 M_\odot$ and $|\vec{v}_{\text{sub}}| = 200$ km/s was assumed, along with $n_\star = 5 \cdot 10^3$ kpc $^{-3}$ and $\sigma_x = \sigma_y = \sigma_z = 100/\sqrt{2}$. Larger M_{sub} , n_\star and lower σ_\star were chosen in generated stellar maps to emphasize the features, since these contain shot noise due to the binning procedure, which makes its harder to observe the characteristic patterns by eye. The green dashed circle (and dot in the left hand side plot) only serve as a guidance for the location of the subhalo, whose centre lies at $x = 0$ and $y = 0$.

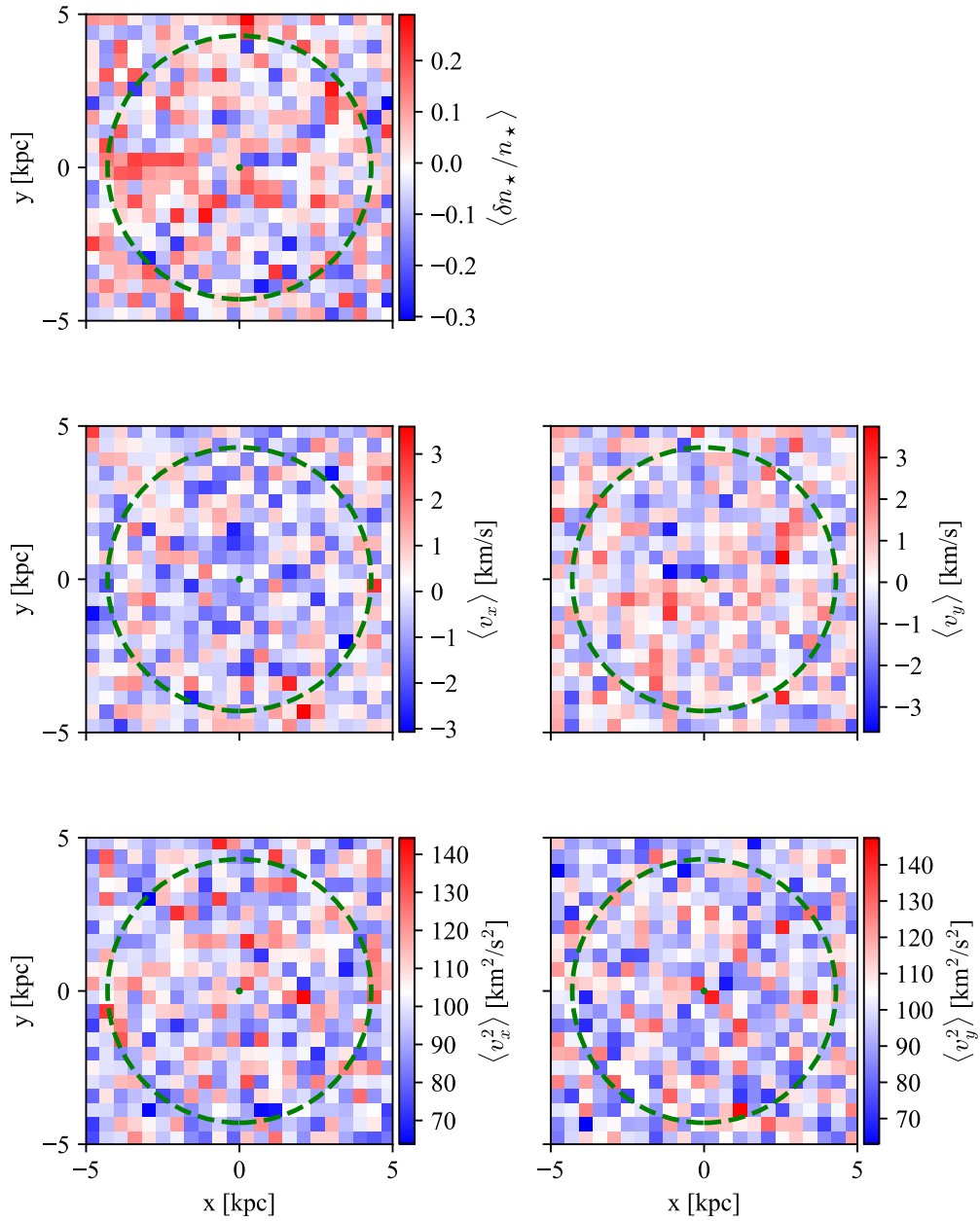


Figure 3: Bin-averaged stellar number density and first two moments of their velocity distribution obtained from a mock catalog with a single DM subhalo of $M_{\text{sub}} = 10^7 M_\odot$, moving in the positive \hat{x} direction with 100 km/s. The fiducial values of stellar parameters are $n_\star = 10^3 \text{ kpc}^{-3}$ and $\sigma_\star = 10 \text{ km/s}$, while green circle marks the subhalos range of influence, r_g .

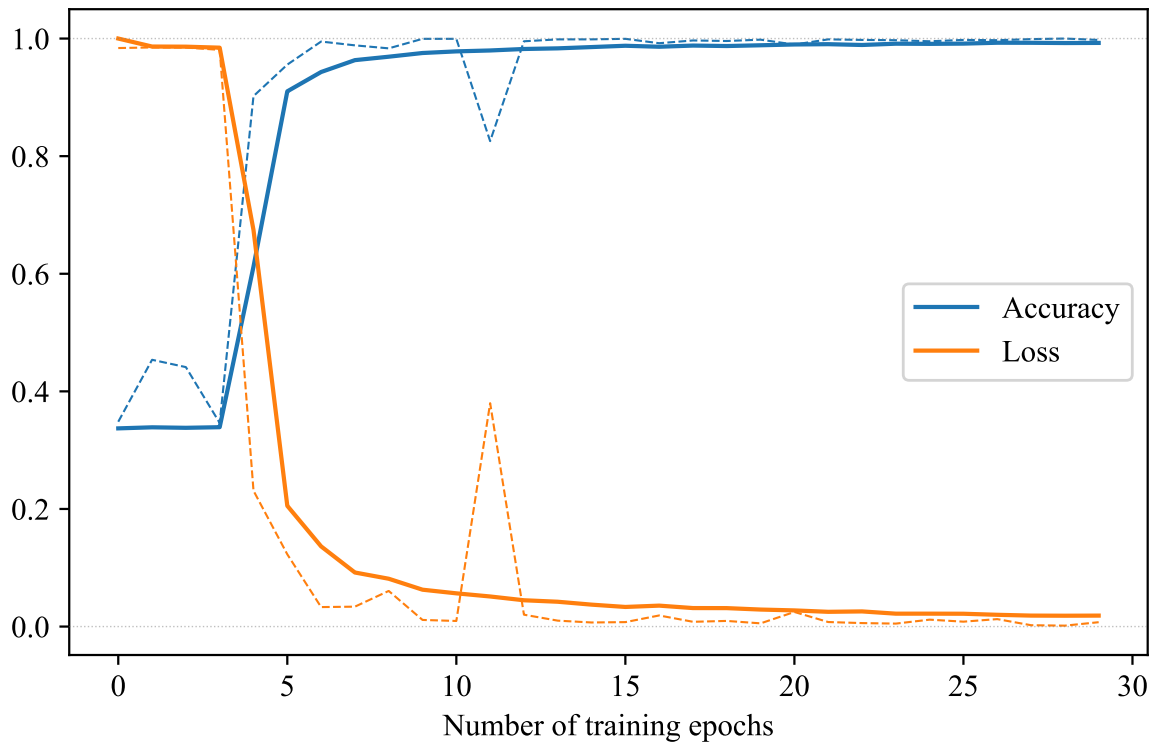


Figure 4: CNN accuracy and normalized loss function for training (solid lines) and validation (dashed lines) datasets as a function of elapsed training epochs. The above results were obtained for homogeneous isotropic stellar field with $n_{\text{sub}} \in [0, 2]$ point-masses of $M_{\text{sub}} = 10^7 M_{\odot}$ and stellar field with $n_{\star} = 10^3 \text{ kpc}^{-3}$ and $\sigma_{\star} = 10 \text{ km/s}$.

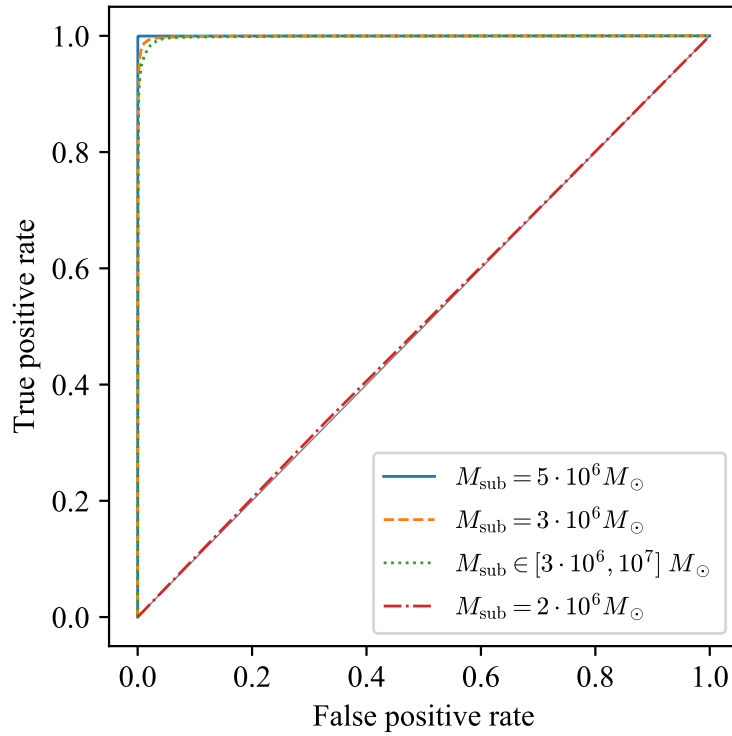


Figure 5: ROC (receiver operating characteristic) curves for CNNs trained on datasets with different subhalo masses M_{sub} , but same fiducial stellar field parameters, namely $n_{\star} = 10^3 \text{ kpc}^{-3}$ and $\sigma_{\star} = 10 \text{ km/s}$.

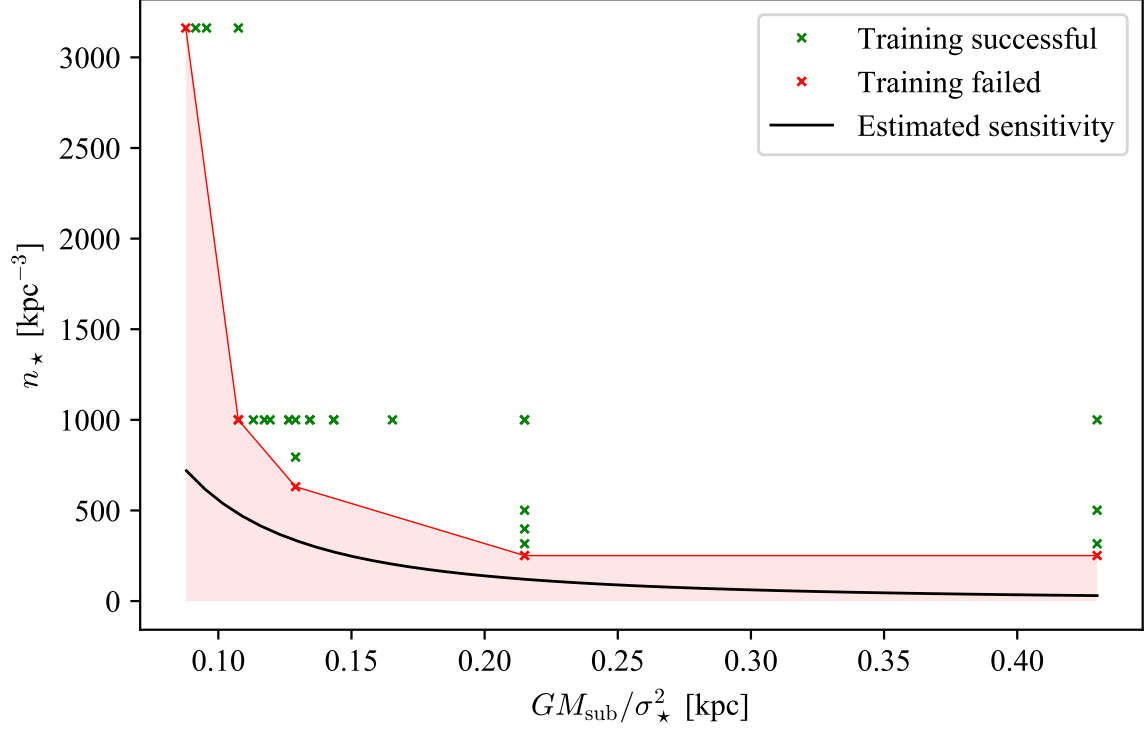


Figure 6: The ability of CNN to successfully train at given point in the subhalo mass over stellar velocity dispersion, $GM_{\text{sub}}/\sigma_{\star}^2$, versus stellar number density, n_{\star} , plane. Green crosses mark the points where network successfully trained and reach accuracy above 95%, while red crosses mark the points where network failed to train, resulting in accuracy $\sim 33\%$. The red region marks the part of parameter space, where the CNN approach is expected to fail, while the black line denotes the sensitivity threshold estimate from equation (4), assuming $\delta v_{\star} \ll \sigma_{\star}/\sqrt{N_b}$.